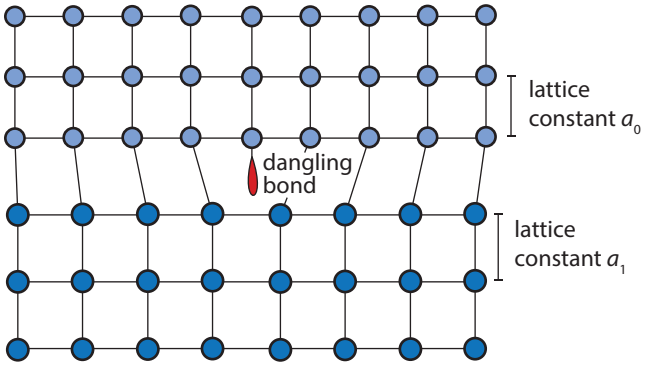

Figure 13.11: Illustrating the lattice mismatch at an interface between two different III-V materials.

of 1.8 eV material and with matching lattice constant. Consequently, triple junction cells based on GaInP, GaAs and Germanium can be fully lattice matched.

13.3 Thin-film silicon technology

In this section we will discuss thin-film silicon solar cells, which can be deposited on glass substrates and even on flexible substrates.

13.3.1 Thin-film silicon alloys

Thin-film silicon materials usually are deposited with *chemical vapour deposition* (CVD) processes that we will discuss in more detail in Section 13.3.3. In chemical vapour deposition different *precursor gasses* are brought into the reaction chamber. Due to chemical reactions, layer is formed on the substrate. Depending on the used precursors and other deposition parameters such as the gas flow rate, pressure, and temperature, various different alloys with different electrical and optical parameters can be deposited. We will discuss the most important alloys in the following paragraphs.

We start with two alloys consisting of silicon and hydrogen: *hydrogenated amorphous silicon* (a-Si:H) and *hydrogenated nanocrystalline silicon* (nc-Si:H), which is also known as microcrystalline silicon. The term *hydrogenated* indicates that some of the valence electrons in the silicon lattice are *passivated* by hydrogen, which is indicated by the ':H' in the abbreviation. The typical atomic hydrogen content of these alloys is from 5% up to about 15%. The hydrogen passivates most defects in the material, resulting in a defect density around 10^{16} cm^{-3} [66], which is suitable for PV applications. Often, the term 'hydrogenated' is left out for simplicity. Pure amorphous silicon (a-Si) would have an extremely high defect density ($> 10^{19}$ cm^{-3}) [67], which would result in fast recombination of photo-excited excess carriers. Similarly, we can make alloys from *germanium* and hydrogen: *hydrogenated amorphous germanium* (a-Ge:H) and *hydrogenated nanocrystalline germanium* (nc-Ge:H).

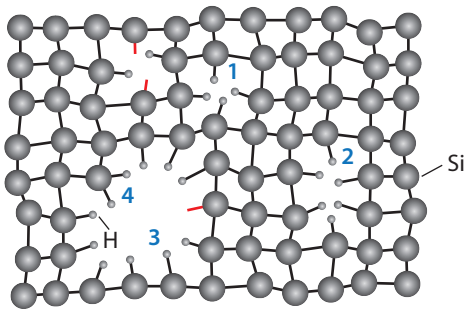

Figure 13.12: Illustrating the atomic structure of amorphous silicon with four typical defects: (1) monovacancies, (2) divacancies, (3) nanosized voids with mono- and (4) dihydrides. With kind permission of M. A. Wank [68].

Let us now take a look at alloys of silicon with four valence electrons with other elements with four valence electrons, *carbon and germanium*. In thin-film silicon solar cells, both hydrogenated amorphous and nanocrystalline *silicon-germanium alloys* (a-SiGe:H and nc-SiGe:H) are being used. Silicon is also mixed using the four valence electron material, carbon, leading to hydrogenated amorphous *silicon carbide* (a-SiC:H).

Another interesting alloy is obtained when oxygen with six valence electrons is incorporated into the lattice: *hydrogenated nanocrystalline silicon oxide* is often used in thin-film silicon solar cells.

All these alloys can be doped, usually boron is used as a p dopant while phosphorus is the most common n dopant.

Many of the alloys mentioned above are present as *amorphous* materials. It is hence important to discuss the structure of amorphous lattices. In this discussion we will limit ourselves to amorphous silicon, since it is the best studied amorphous semiconductor and the general properties of the other amorphous alloys are similar. In Chapter 12 we thoroughly discussed crystalline silicon, which has an ordered lattice in which the orientation and structure is repeated in all directions. For amorphous materials this is not the case, but the lattice is disordered as it is illustrated in Fig. 13.12. This figure shows a so-called *continuous random network* (CRN). On atomic length scales, or also called *short-range order*, the atoms still have a tetrahedral coordination structure, just like crystalline silicon. But the silicon bond angles and silicon-silicon bond lengths are slightly distorted with respect to a crystalline silicon network. However, at larger length scales, or also referred to as long range, the lattice does not look crystalline anymore. Not all silicon atoms have four silicon neighbours, but some valence electrons form dangling bonds, similar to the unpassivated surface electrons already discussed in Chapter 12. Recent studies show that these dangling bonds are not distributed homogeneously throughout the amorphous lattice, but that they group in divacancies, multivacancies or even nanosized voids [69]. The surfaces of these volume deficiencies are passivated with hydrogen. mets

Another phase of hydrogenated silicon alloys is the *nanocrystalline* phase with a structure even more complex than in amorphous materials. Nanocrystalline hydrogenated silicon consists of small grains that have a crystalline lattice and are a few tens of nanometres big. These grains are embedded in a tissue of hydrogenated amorphous silicon. Figure

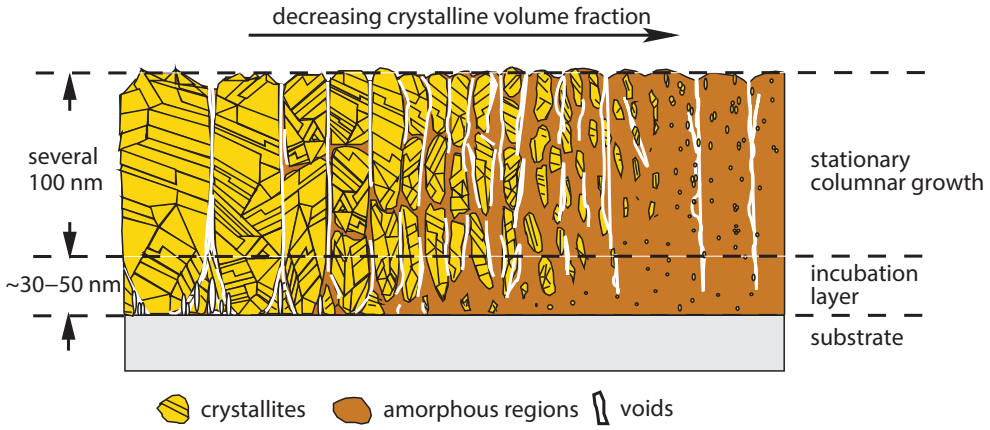

Figure 13.13: The various phases of thin-film silicon with a highly crystalline phase on the left and amorphous silicon on the right [70, 71].

13.13 shows the various phases of thin-film silicon [70, 71]. On the left-hand side, a fully crystalline phase is shown, which is close to that of poly-crystalline silicon, except that is has much more cracks and pores in it. On the right hand side, the phase represents the amorphous lattice. Please note again, that the terms microcrystalline and nanocrystalline refer to the same material. Going from right to left, the amorphous phase is changing into a mixed phase with a few small crystalline grains to a phase which is dominated by large crystalline grains and a small fraction of amorphous tissue. Research has shown that the best nanocrystalline bulk materials used in solar cells have a network close to the *amorphous-nanocrystalline silicon transition region* and its crystalline volume fraction is in the order of 60%.

The bandgap of nanocrystalline silicon is close to that of crystalline silicon ($\approx$ 1.12 eV) due to the crystalline network in the grains. The bandgap of amorphous silicon is in the order of 1.6 up to 1.8 eV, which can be tuned by the amount of hydrogen incorporated in to the silicon network. It is larger than that of crystalline silicon because of the distortions in bond angles and bond lengths. It is out of the scope of this book to discuss the reasons for this increase in bandgap in more detail. An important consequence of a disordered amorphous lattice is that the electron momentum is poorly defined in contrast to crystalline silicon. As we discussed in Chapter 12, both energy and momentum transfer are needed to excite and electron from the valence band to the conduction band. Hence, crystalline silicon is an indirect bandgap material. This is not true for amorphous silicon, which is a direct bandgap material. Therefore the absorptivity of a-Si:H is much higher than that of c-Si, as we can see in Fig. 13.14. We see that the absorption coefficient for amorphous silicon in the visible spectrum is much larger that that of crystalline silicon. In some wavelength regions it is about two orders of magnitude larger, which means that much thinner silicon films can be used in reference to the typical wafers in crystalline silicon solar cells. In the figure, also data for amorphous silicon-germanium are shown. a-SiGe:H has lower bandgap and even higher absorption coefficient in the visible. Its bandgaps are in the range of 1.4 up to 1.6 eV. Amorphous silicon carbide alloys have bandgaps of 1.9 eV and

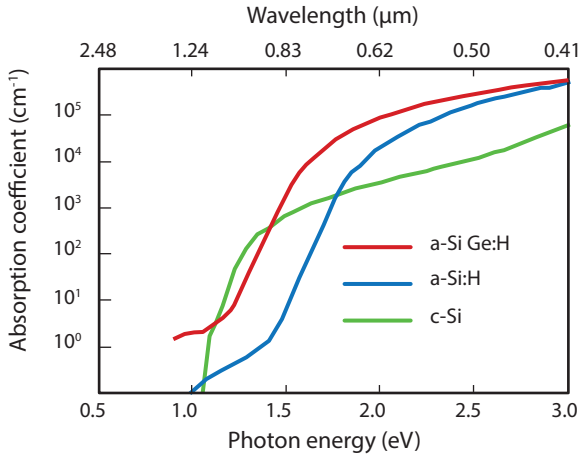

Figure 13.14: The absorption coefficients of different thin-film silicon materials.

larger. Finally, nanocrystalline silicon oxides have bandgaps exceeding 2 eV.

13.3.2 The design of thin-film silicon solar cells

The first successful a-Si:H solar cell with an efficiency of 2.4% was reported by Carlson and Wronski in 1976 [72]. We now will discuss how such solar cells can be designed and what are the issues in designing them.

When compared to c-Si, hydrogenated amorphous and nanocrystalline silicon films have a relatively high defect density of around 10^{-16} cm^{-3}. As mentioned before, because of the disordered structure not all valence electrons are able to make bonds with the neighbouring atoms. The dangling bonds can act as defects that limit the lifetime of the light excited charge carriers. This is described with Shockley-Read-Hall recombination, which controls the diffusion length. Because of the high defect density the diffusion length of charge carriers in hydrogenated amorphous silicon is only 100 nm up to 300 nm. Hence, the transport of charge carriers in a thick absorber can not rely on diffusion.

Therefore, amorphous silicon solar cells are *not* based on a *p*-*n* junction like wafer based c-Si solar cells. Instead, they are based on a *p*-*i*-*n* junction, which means that an intrinsic (undoped) layer is sandwiched between thin *p*-doped and *n*-doped layers, as illustrated in Fig. 13.15 (a). While the *i*-layer is several hundreds of nanometres thick, the doped layers are only about 10 nm thick. Between the *p*- and *n*-doped layers a built-in electric field across the intrinsic absorber layer is created. This is illustrated in the electronic band diagram shown in Fig. 13.15 (b). If the layers are not connected to each other, the Fermi level in the *p*- *n* layers is closer to the valence and the conduction bands, respectively. For the intrinsic layer, it is in the middle of the bandgap. When the *p*, *i*, and *n* layers are connected to each other, the Fermi level has to be the same throughout the junction, if it is in the dark and under thermal equilibrium. This creates a slope over the electronic band in the intrinsic film as we can see in the illustration. This slope reflects the built-in electric field.

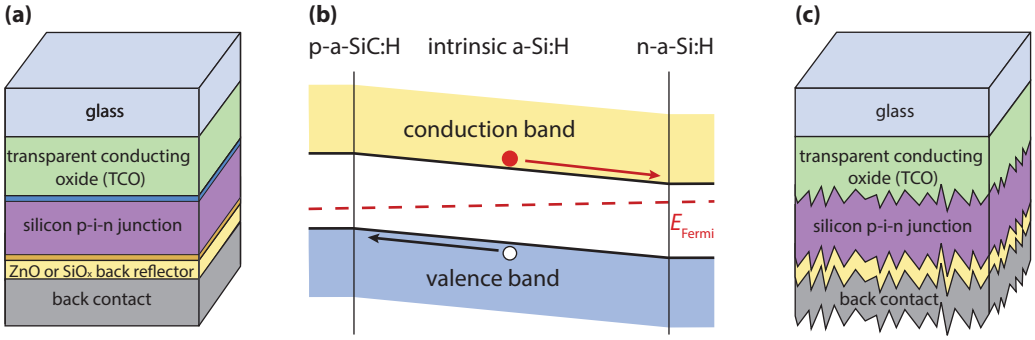

Figure 13.15: Illustrating the (a) layer structure and the (b) band diagram of an amorphous silicon solar cell. (c) Thin-film silicon solar cells have nanotextured interfaces.

Another way to look at the field is to consider the *i*-layer as an dielectric in between to charged plates (the doped layers). Neglecting edge effects, the electric field in the *i* layer is given by

$$E = \frac{\sigma}{\epsilon\epsilon_0}, \tag{13.6}$$

where σ is the charge density on the doped layers and ϵ is the electric permittivity of the *i*-layer material. Note that the electric field in the *i* layer is constant. Following Eq. (4.29), we find the voltage in the *i* layer to be

$$V(x) = -\int E(x)\,\mathrm{d}x = V_0 - \frac{\sigma}{\epsilon\epsilon_0}x. \tag{13.7}$$

We see that the voltage and hence the energy in the *i* layer is linear, just as shown in the band diagram of Fig. 13.15 (b).

Because of the electric field, the light excited charge carrier will move through the intrinsic layer. As discussed in Section 6.5.1, the holes move up the slope in the valence band towards the *p* layer and the electrons move down the slope in the conduction band towards the *n* layer. Such a device, where electronic drift because of an electric field is the dominant transport mechanism is called a *drift device*. In contrast, a wafer based crystalline silicon solar cell, as discussed in Chapter 12, can be considered as a *diffusion device*.

Note, that because of the intrinsic nature of the absorber layer the hole and electron density is in the same order of magnitude. On the other hand, in the *p* layer the holes are the majority charge carriers and the dominant transport mechanism is diffusion. Similarly, in the *n* layer the electrons are the majority charge carriers and again diffusion in the dominant transport mechanism. Because of the low diffusion length, both *p* and *n* layers must be very thin.

Now we take another look at Fig. 13.15 (a). The cell sketched there is deposited in *superstrate* configuration. This means that the layer that is passed first by the incident light in the solar cell is also deposited first in the production process. Also the term *p-i-n* layer refers to this superstrate configuration, as it indicates the order of the depositions: because in thin-film silicon holes have a significantly lower mobility than electrons, the *p* layer is

in front of the *n* layer and hence the *p* layer is deposited first. As then the generation rate is higher close to the *p* layer, more holes can reach it.

In superstrate thin-film silicon solar cells, usually glass is used as a superstrate because it is highly transparent and can easily handle all the chemical and physical conditions in that all the depositions are carried out. Before the *p-i-n* layers can be deposited, a *transparent front contact* has to be deposited. Usually *transparent conducting oxides* are used, that we introduced in Section 13.1.

Another possible configuration is the *substrate configuration*. There, either the substrate acts like a back contact or the back contact is deposited on the substrate. Consequently, no light will pass through the substrate. Thin-film silicon solar cells deposited in the substrate configuration are also called *n-i-p* cells as the *n* layer is deposited before the *i* layer and the *p* layer.

Usually, thin-film silicon solar cells have no flat interfaces, as shown in Fig. 13.15 (a), but nano-textured interfaces, as illustrated in Fig. 13.15 (c). These textured interfaces scatter the incident light and hence prolong the average path length of the light through the absorber layer. Therefore, more light can be absorbed and the photocurrent can be increased. This is an example of *light management* that we discussed in Section 10.4.3.

Often, the *p* layer is not made from amorphous silicon. Instead, materials with a higher bandgap are used, such as silicon carbide or silicon oxides in order to minimise *parasitic absorption* mainly in the blue part of the spectrum. Usually, boron is used as a dopant. Also for the *n* layer often silicon oxides are used, but sometimes still a-Si:H is utilised with phosphorus being the main dopant. The *n*-SiO_x:H is very transparent. Therefore it also can be used as a back reflector structure when its thickness is chosen such that destructive interference occurs at the *i-n* interface minimising the electric field strength and hence parasitic absorption in the *n* layer. Additionally, also several tenth of nm thick TCO can be used with the same purpose. Further, a metallic back reflector that also acts as the electric back contact is used. Because of its attractive cost, mainly aluminium is used for this purpose. However, also silver that has a higher reflectivity can be used, yet is it more expensive.

The bandgap of hydrogenated amorphous silicon is in the order of 1.75 eV, hence it only is absorptive for wavelength shorter than 700 nm. The highest current densities achieved in single junction amorphous silicon solar cell are 17 up to 18 $mA \cdot cm^{-2}$, whereas the maximum theoretic current that could be achieved up to 700 nm is in the order of 23 $mA \cdot cm^{-2}$. Thus, the EQE averaged over the spectrum is in the order of 74 to 77%.

The highest achieved open circuit voltages are in the order of 1.0 eV. With respect to a bandgap of 1.75 eV the bandgap utilisation is quite low because of the high levels of Shockley-Read-Hall recombination and the relatively broad valence and conduction-band tails. The highest stabilised efficiency of single junction solar cells is 10.1% [47]. It was obtained by the research Oerlikon Solar Lab in Switzerland, which currently is a subsidiary of the Japanese Tokyo Electron Ltd.

Besides a-Si:H, also nanocrystalline silicon films are used for the intrinsic absorber layers in *p-i-n* solar cell as well. The spectral utilisation of the nc-Si:H is better than that of amorphous silicon because of the lower bandgap of nc-Si:H. However, to utilise the spectral part from 700 up to 950 nm, thicker films are required, because of the indirect bandgap of the silicon crystallites. Typical intrinsic film thicknesses are in between 1 µm and 3 µm. The current nc-Si:H record cell has a short circuit current density of 28.8 $mA \cdot cm^{-2}$, an open

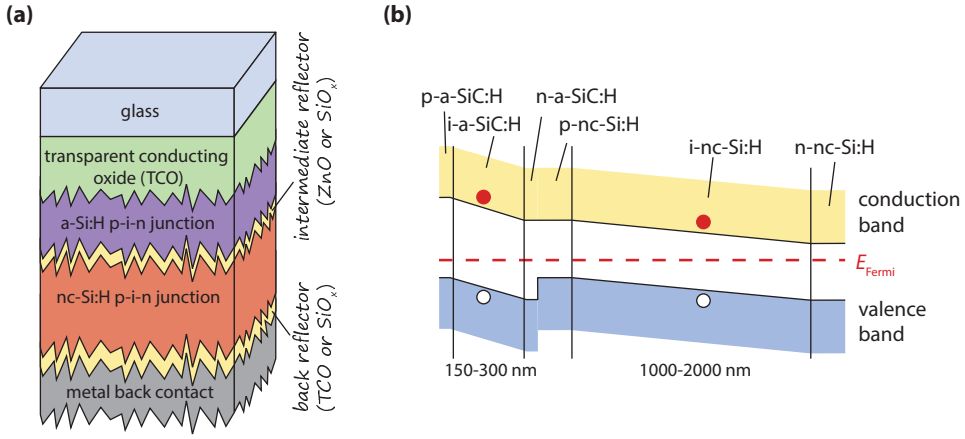

Figure 13.16: Illustrating the (a) layer structure and the (b) band diagram of a micromorph silicon solar cell.

circuit voltage of 523 mV and an efficiency of 10.8% [47]. This result was achieved by the *Japanese Institute of Advanced Industrial Science and Technology* (AIST).

Neither a-Si:H nor nc-Si:H has an optimal spectral utilisation. Therefore also in thin-film technology the *multi-junction* approach is used, just like for III-V solar cells. Probably the most studied concept is the *micromorph* concept illustrated in Fig. 13.16 (a), which is a double junction concept consisting of an a-Si:H and a nc-Si:H junction. Like before, the solar cell with the highest bandgap is used as a top cell that converts the most energetic photons into electricity, while the lower bandgap material is used for the bottom cell and converts the lower energetic photons.

Figure 13.16 (b) shows the typical band diagram of such a micromorph solar cell, that is also called a *tandem solar cell*. On the left hand side the electronic band diagram of the amorphous silicon top cell is shown; on the right hand side the electronic band diagram of nanocrystalline silicon bottom cell is shown. The blue and green short-wavelength light is absorbed in the top cell, where electron-hole pairs are generated. Similarly, the red and infrared long-wavelength light is absorbed in the bottom cell, where also electron-hole pairs are generated. Let us take a closer look on the two electron-hole pairs excited in the top and bottom cells, respectively. The hole generated in the amorphous top cell moves to the top *p* layer and the electron excited in the bottom cell drifts to the bottom *n* layer. Both can be collected at the front and back contacts. However, the electron excited in the top cell drifts to the top *n* layer and the hole generated in the bottom cell drifts to the *p* layer. Just as for the III-V multi-junction devices, the electrons and holes have to recombine at a *tunnel recombination junction* between the *n* layer of the top cell and the *p* layer of the bottom cell. Often a very thin and defect rich layer is used for this purpose. Just as for the III-V multi-junction solar cells, the total current density is equal to that of the junction with the lowest current density. Therefore, for an optimised multi-junction cell all current densities in the various sub cells have to be matched in order to achieve the best spectral utilisation.

Figure 13.17 shows the *J-V* curves of a single junction a-Si:H solar cell and of a single

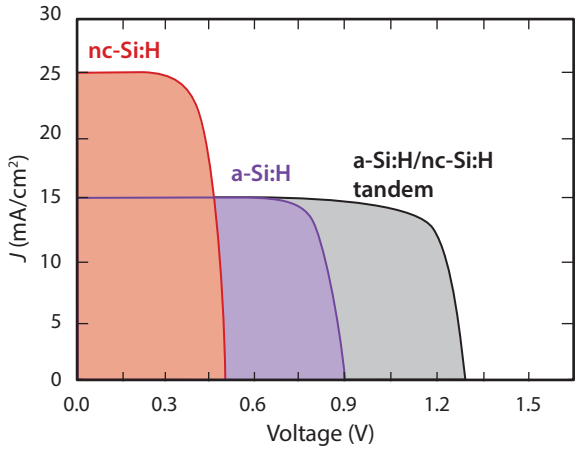

Figure 13.17: The *J-V* curve of a micromorph solar cell and its isolated subcells.

junction nc-Si:H solar cell. Let us assume that the V_{oc} of the high bandgap a-Si:H top cell has an open circuit voltage of 0.9 V and a relatively low short circuit density of 15 mA·cm^{-2}, whereas the low bandgap material of nc-Si:H has a lower open circuit voltage of 0.5 volt and a higher short circuit current density of 25 mA·cm^{-2}. If we make a tandem of both junctions, the resulting current density of the double junction is lower than the currents in both bottom cells. Because the open circuit voltage is approximately proportional to $\ln(J_{ph}/J_0)$, the open circuit voltages of the junctions in a tandem cell will be slightly lower than for similar single junction cells. The total current utilisation of the tandem cell is determined by the bottom cell, *i.e.* 25 mA·cm^{-2}. Given the examples of the single junctions here, the best current density matching of both cells would deliver 12.5 mA·cm^{-2}. The current tandem record cell has an efficiency of 12.3% and was manufactured by the Japanese company *Kaneka* [47].

Just as for the III-V technology, also with thin-film technology multi-junction cells with more than two junctions can be made. For example the former US company *United Solar Ovonic LLC* made a thin-film silicon based triple junction device with an a-Si:H top cell, an a-SiGe:H middle cell and a nc-Si:H bottom cell, illustrated in Fig. 13.18 (a). As illustrated in this figure, also various other combinations for triple junctions can be made, for example a-Si:H/nc-Si:H/nc-Si:H. Figure 13.18 (b) shows the spectral utilisation[3] of the three junctions and the total cell of the record device by United Solar. In contrast to the EQE of the multi-junction III-V cell (Fig. 13.9), where the EQEs of the individual cells are block functions, here the individual EQEs show various overlaps: light with wavelengths below 450 nm is utilised by the top cell only, light at around 550 nm is utilised by the top and middle cells, light at around 650 nm is utilised by all three junctions, and light above 900 nm is utilised by the bottom cell only. Consequently, optimising thin film silicon multi-junction solar cells is a complex interplay between the various absorber thicknesses and light management concepts. The *initial efficiency* of the current record triple junction cell by Uni Solar Ovonic is 16.3%.

[3] The spectral utilisation is given as EQE·AM1.5.

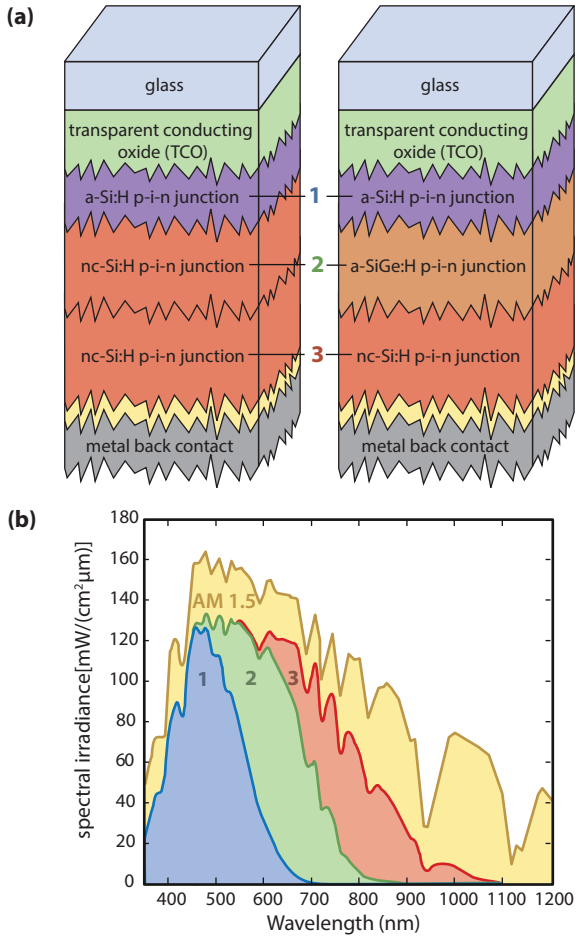

Figure 13.18: (a) Two possible structures and (b) the typical spectral utilisation (EQE·AM1.5) of a triple-junction thin-film silicon cell.

The term *initial* refers to a big issue for amorphous thin-film silicon alloys: they suffer from *light induced degradation* which leads to a reduction of the efficiency. For example, for the initial 16.3% record cell the efficiency drops below the 13.4% of the current *stabilised* record cell. This record cell consists of an a-Si:H/nc-Si:H/nc-Si:H stack and was produced by the South Korean *LG Corp.* [47].

Light induced degradation, which is also referred to as the *Staebler-Wronski effect* (SWE), is one of the biggest challenges for thin-film solar cells. It was already discovered one year after the first a-Si:H solar cells were made in 1977 [73]. Because of the recombination of light excited charge carriers, *meta-stable* defects are created in the absorber layers. The increased defect density leads to increased bulk charge carrier recombination, which mainly affects the performance of the amorphous solar cells. After about 1000 hours of illumination, the efficiency of amorphous thin-film solar cells stabilises at around 85% - 90% of the initial efficiency and stays stable for the rest of its lifetime. If the SWE could be tackled, thin-film silicon devices easily could achieve stable efficiencies well above 16%.

Just as for III-V cells, current density matching is very important for thin-film silicon multi-junction cells. First, nanotextured surfaces scatter the incident light in order to enhance the average photon path length and hence to increase the absorption in the various absorber layers of the multi-junction cell. Scattering becomes more important for the bottom cell because its nc-Si:H film is the thickest layer in the device has to absorb most of the red and infrared, where nc-Si:H is not that absorptive. Secondly, intermediate reflector layers are used as a tool to redistribute the light between the junctions above and below them. More specifically, the top and bottom junctions are separated with a low reflective index material, such as nc-SiO_x:H. Because of the refractive index difference of the top absorber and the nc-SiO_x:H, more light is reflected back into the top cell. Thus, the a-Si:H top cell can be made thinner, which makes it less sensitive to light-induced degradation.

13.3.3 Making thin-film silicon solar cells

To get a better understanding of fabricating thin-film silicon solar cells, we take a look at the production process used at the Else Kooi Laboratory in Delft, the Netherlands. Before the deposition can start, the sample has to be cleaned in a *ultrasonic cleaning bath.* During cleaning, dirt and dust particles are removed, which could lead to a *shunt* between the front and back contact in the final solar cell. Now, the TCO layer can be deposited. In Delft, we can deposit ZnO:Al or ITO with sputtering processes. After sputtering, ZnO:Al can be etched with acids in order to achieve a crater-like structure for light scattering. Alternatively, the sample can already be covered with a TCO layer, for example SnO_2:F from the Japanese *Asahi* company, which already has a pyramid-like structure for light scattering because of its deposition process. Also on SnO_2:F a 5-10 nm thick ZnO:Al layer is deposited that protects the SnO_2:F from being reduced by hydrogen-rich plasma present during the deposition of the thin-film silicon layers. During sputtering, the zinc oxide target is bombarded using an ionised noble gas like Argon. The generated aluminium zinc oxide species are sputtered into the chamber and deposited on to the substrate.

Before the thin-film silicon layers are deposited, a thin Al strip is deposited on the side of the sample, that will act as electric front contact when the cells are measured.

Processing of the different thin-film silicon layers often happens in multi-chamber setups that allow to process each layer in a separate chamber and therefore can prevent cross-

contamination, *e.g.* from *p* and *n* dopants, which would reduce the quality of the layers. After the sample is mounted on a suitable *substrate holder*, it enters the setup via a *load lock*, in which the substrate is brought under low pressure before it's moved into the processing chambers. This avoids the processing chambers to be contaminated with various unwelcome atoms and molecules present in ambient air. Then the sample is brought into a central chamber, from where all process chambers can be accessed.

The typical precursor gas for depositing the Si films is silane (SiH_4), often diluted with hydrogen (H_2). The precursor gasses are brought into the process chamber at low pressure. In plasma enhanced chemical vapour deposition (PE-CVD), a radio-frequency (RF) or very-high-frequency (VHF) bias voltage between two electrodes is used to generate a plasma, which leads to dissociation of the SiH_4 atoms into radicals such as SiH_3, SiH_2 or SiH. This radicals react with the substrate, where a layer is growing. By increasing the H_2 content, the material becomes more nanocrystalline, as sketched in Fig. 13.13.

As precursors for the doping, mainly diborane (B_2H_6) is used for *p* layers and phosphine (PH_3) is used for the *n* layers. For silicon carbide layers, additionally to the silane, methane (CH_4) is used. Silicon oxide layers can be made by combining silane with carbon dioxide (CO_2).

After the *p-i-n* junction is deposited, the sample is covered with a *mask*, which defines the areas on that the metallic back contacts are deposited. In Delft, silver is deposited with *evaporation*. Little pieces of silver are put in a boat that is heated by a very high current flowing through it. The silver melts and evaporated silver particles can move freely through a vacuum until they hit the sample, where a silver layer is deposited. This process is explained in more detail in Chapter 14.

Now the solar cells are ready — every metallic square defines a little solar cell. The small metal strip is the front contact and the back of the metallic square is the electric back contact. Naturally, such a configuration is not suitable for large-scale thin-film PV modules. The production of thin-film modules is discussed in Chapter 15.

13.3.4 Crystalline silicon thin-film solar cells

We conclude the section on thin-film silicon technology with a brief discussion on *crystalline silicon thin-film solar cells*. The aim is to combine the advantages of crystalline silicon technology and thin-film silicon technology [74] by using high-quality crystalline films of only several tenths of micrometers thickness as absorbers. These films are positioned on a substrate or a superstrate.

Different approaches are investigated for reaching this goal: Kerf-less wafering techniques are investigated where thin wafers can be prepared without any kerf loss. The wafers then are transferred on a glass substrate. With this technique, efficiencies of 10.0% were obtained with a 50 µm thick absorber [74].

Alternatively, films of large-grain nanocrystalline silicon or amorphous silicon can be deposited. The amorphous films can be crystallised after deposition. This crystallisation process can be categorised between *solid-phase* (SPC) and *liquid-phase* crystallisation (LPC). SPC can be done for example in a thermal annealing step. Because of the low electrical quality of the defect-rich SPC silicon films, the maximally achieved efficiency is 10.5% and was achieved by the company CSG Solar [74]. In LPC, the amorphous Si film is molten using e.g. an electron beam or a laser. Then, the molten silicon re-crystallises with grain sizes

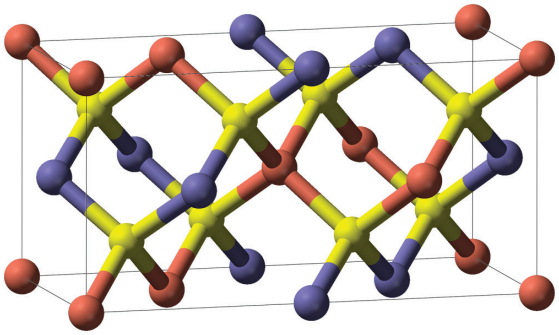

Figure 13.19: The crystal structure of *copper indium diselenide*, a typical chalcopyrite. The colors indicate copper (red), selenium (yellow) and indium (blue). For *copper gallium diselenide*, the In atoms are replaced by Ga atoms [78].

up to several centimetres in growth direction and up to several millimetres orthogonal to the growth direction. These large grains lead to open-circuit voltages comparable to that of wafer-based Si solar cells with reported maximum values of 656 mV [75] and efficiencies of 11.8% have been demonstrated [76].

The highest efficiencies are reached with silicon layers grown in an epitaxy process, just as for the high-performance III-V solar cells. The epitaxy films then are transferred on glass. The current record cell made with this method has an efficiency of 20.1% on a 43 µm thick substrate and was fabricated by the American company SOLEXEL [77].

13.4 Chalcogenide solar cells

The third class of thin-film solar cells that we discuss are the large class of *chalcogenide solar cells*, where our focus mainly will be on CIGS and cadmium telluride (CdTe) solar cells. The term *chalcogenides* refers to all chemical compounds consisting of at least one *chalcogen* anion from the group 16 (also known as *group VI*) with at least one or more electropositive elements. Five elements belong to group 16: oxygen (O), sulphur (S), selenium (Se), tellurium (Te), and the radioactive polonium (Po). Typically, oxides are not included in discussions of chalcogenides. Because of its radioactivity, compounds with Po are of only very limited relevance for semiconductor physics.

13.4.1 Chalcopyrite solar cells

The first group of chalcogenide solar cells that we discuss are *chalcopyrite solar cells*. The name of this class of materials is based on *chalcopyrite* (copper iron disulphide, $CuFeS_2$). Like all the chalcopyrites, its forms *tetragonal* crystals, as illustrated in Fig. 13.19.

Many chalcopyrites are semiconductors. As they consist of elements from groups I, III, and VI, they are also called I-III-VI semiconductors or *ternary* semiconductors. In principle,